

Denoising Multi-Color QR Codes and Stiefel-Valued Data by Relaxed Regularizations

Robert Beinert* Jonas Bresch†

July 1, 2025

Abstract

The handling of manifold-valued data, for instance, plays a central role in color restoration tasks relying on circle- or sphere-valued color models, in the study of rotational or directional information related to the special orthogonal group, and in Gaussian image processing, where the pixel statistics are interpreted as values on the hyperbolic sheet. Especially, to denoise these kind of data, there have been proposed several generalizations of total variation (TV) and Tikhonov-type denoising models incorporating the underlying manifolds. Recently, a novel, numerically efficient denoising approach has been introduced, where the data are embedded in an Euclidean ambient space, the non-convex manifolds are encoded by a series of positive semi-definite, fixed-rank matrices, and the rank constraint is relaxed to obtain a convexification that can be solved using standard algorithms from convex analysis. The aim of the present paper is to extend this approach to new kinds of data like multi-binary and Stiefel-valued data. Multi-binary data can, for instance, be used to model multi-color QR codes whereas Stiefel-valued data occur in image and video-based recognition. For both new data types, we propose TV- and Tikhonov-based denoising models together with easy-to-solve convexification. All derived methods are evaluated on proof-of-concept, synthetic experiments.

Keywords— Denoising of multi-binary valued data, manifold-valued data, signal and image processing on graphs, total variation, Tikhonov regularization, convex relaxation.

2020 AMS Mathematics Subject Classification— 94A08, 94A12, 65J22, 90C22, 90C25

1 Introduction

Due to novel emerging acquisition techniques, data processing on manifold-valued signals and images becomes more and more important. Especially, when the data manifold is non-convex, classical data processing tasks like denoising turn into challenging novel problems. In real-world applications, data with values on non-convex manifolds, for instance, play a major role in color restoration tasks relying on the HSV (hue-saturation-value) or LCh (lightness-chromaticity-hue) color space [20, 25], where the hue is

*R. Beinert is with the Institute of Mathematics, Technische Universität Berlin, Straße des 17. Juni 136, 10623 Berlin, Germany.

†J. Bresch is with the Institute of Mathematics, Technische Universität Berlin, Straße des 17. Juni 136, 10623 Berlin, Germany.

represented by a circle, and the color component is thus interpreted as circle-valued data. For denoising tasks relying on the chromaticity-brightness model [26, 27], the pixels of an image instead attain values on the sphere. Rotation and directional information are modeled using the special orthogonal group; hence the corresponding data are often $\text{SO}(2)$ - or $\text{SO}(3)$ -valued [1, 3]. For Gaussian image processing, mean and variance of the pixel statistic can be interpreted as points on the hyperbolic sheet yielding hyperbolic-valued data [10, 22]. To deal with data of these kinds, especially in the context of denoising, the classic variational Tikhonov and total variation (TV) models have been generalized relying on non-convex optimization methods on the underlying manifolds [8, 9, 13, 17, 19, 21, 23]. All these methods come with some limitations, they either increase the dimension using lifting techniques, require a tree structure of the graph where the data is living on, or are based on a subclass of the considered manifolds. A completely novel approach is proposed in [5–7], where the manifold-valued data are embedded into an Euclidean ambient space allowing the use of standard denoising models. The non-convex side constrains caused by the non-convex manifolds are moreover encoded by a series of positive semi-definite, fixed-rank matrices. Relaxing the fixed rank results in a convexification of the denoiser model that may be solved using standard algorithms from convex analysis.

The aim of this paper is to extend the proposed encoding and convexification techniques in [5–7] to new types of data, namely multi-binary and Stiefel-valued data. Multi-binary signals with values in $\mathbb{B}_d = \{-1, 1\}^d \subset \mathbb{R}^d$, occur in the context of multi-color QR codes for instance. The main idea behind multi-color QR codes is to increase the information density and information capacity by combining three independent black/white QR codes with respect to the color channels in the RGB (red-blue-green) color model [2, 24, 28]. The modules of the resulting QR codes are colored in black, red, blue, green, cyan, magenta, yellow, and white. Since these colors correspond to the vertices of the RGB color space, rescaling and shifting the color space allow us to interpret multi-color QR codes as \mathbb{B}_3 -valued images. Notice that \mathbb{B}_d is actually no manifold. Nevertheless, the TV methods proposed in [5] can be generalized to handle this kind of data. The Stiefel manifold $\mathbb{V}_d(k)$ consists of all k -tuples of orthonormal vectors in \mathbb{R}^d ; thus the Stiefel manifold figuratively consists of all orthogonal bases of all k -dimensional subspaces of \mathbb{R}^d , where the order of the basis vectors matter. The Stiefel manifold arises in image and video-based recognition [29]. The handling orthonormal constraints is, for instance, studied [14, 30], where geodesic- and lifting processes play a major part. In the following, we consider general signals supported on a connected, undirected graph $G = (V, E)$, where $V := \{1, \dots, N\}$ is the set of vertices and $E := \{(n, m) : n < m\} \subset V \times V$ the set of edges, encoding the structure of the data. We set $M := |E|$ to be the number of edges.

This paper is organized as follows: In § 2 we derive a convex relaxation for a \mathbb{B}_d -valued TV denoising model and a numerical solver based on the Alternating Direction Method of Multipliers (ADMM). In Theorem 2, we show that our convexification is actually tight, meaning that every solution of the convexified model can be used to easily construct a solution of the original non-convex model. The denoising of $\mathbb{V}_d(k)$ -valued data is studied in § 3, where we propose a TV model for denoising cartoon-like or piecewise constant data and a Tikhonov model for denoising smooth data. For both variational denoising models, we again derive numerical solvers relying on the ADMM. In § 4, we show the success for our proposed methods by applying the resulting algorithms to denoise multi-color QR codes and Stiefel-valued signals.

2 TV Denoising for Multi-Binary Data

The aim of this section is to generalize the TV-denoising model for binary data in [5] to multi-binary data, which, for instance, occurs in the context of multi-color QR codes. More precisely, multi-binary data takes on values in $\mathbb{B}_d := \{-1, 1\}^d \subset \mathbb{R}^d$. For a graph $G := (V, E)$ as introduced in § 1, we are interested in restoring a multi-binary signal $\mathbf{x} := (\mathbf{x}_n)_{n \in V} \subset \mathbb{B}_d$ from noisy measurement $\mathbf{y} := (\mathbf{y}_n)_{n \in V} \subset \mathbb{R}^d$. Taking the piecewise constant or cartoon-like structure of multi-color QR codes into account, we introduce the following TV denoiser:

$$\arg \min_{\mathbf{x} \in \mathbb{B}_d^N} \frac{1}{2} \sum_{n \in V} \|\mathbf{x}_n - \mathbf{y}_n\|_2^2 + \lambda \text{TV}(\mathbf{x}), \quad \text{where} \quad \text{TV}(\mathbf{x}) := \sum_{(n, m) \in E} \|\mathbf{x}_n - \mathbf{x}_m\|_1, \quad (1)$$

which relies on an anisotropic TV regularization on the ambient space \mathbb{R}^d , and where λ is a positive regularization parameter. Since the domain \mathbb{B}_d^N is non-convex, we thus have to solve a non-convex minimization problem. To convexify (1), we first exploit that $\|\mathbf{x}_n\|^2 = 1$ and that $\|\mathbf{y}_n\|^2$ is fixed by the given data; therefore, we have $\frac{1}{2}\|\mathbf{x}_n - \mathbf{y}_n\|_2^2 = -\langle \mathbf{x}_n, \mathbf{y}_n \rangle + \text{constant}$ such that the objective in (1) can be replaced by

$$\mathcal{K}(\mathbf{x}) := - \sum_{n \in V} \langle \mathbf{x}_n, \mathbf{y}_n \rangle + \lambda \text{TV}(\mathbf{x}).$$

Second, we convexify the domain of (1) via replacing \mathbb{B}_d by its convex hull $\mathbb{C}_d := \text{conv}(\mathbb{B}_d) = [-1, 1]^d$, which in fact yields a cube in \mathbb{R}^d . Instead of solving (1), we propose to solve the **convexified TV model**:

$$\arg \min_{\mathbf{x} \in \mathbb{R}^{d \times N}} \mathcal{K}(\mathbf{x}) \quad \text{s.t.} \quad \mathbf{x}_n \in \mathbb{C}_d \quad \forall n \in V. \quad (2)$$

Heuristically, the term $-\langle \mathbf{x}_n, \mathbf{y}_n \rangle$ in the objective \mathcal{K} pushes \mathbf{x}_n in direction \mathbf{y}_n until it hits the boundary

$$\partial \mathbb{C}_d = \{ \boldsymbol{\xi} \in \mathbb{C}_d : \exists i \in \{1, \dots, d\} \text{ s.t. } |\boldsymbol{\xi}_i| = 1 \}$$

and, in the best case, a corner in \mathbb{B}_d .

Tightness of the Convexified TV Model In analogy to binary signals [5], the convexification (2) is in fact tight. This means that every solution of (2) can be used to obtain a solution of the original non-convex problem (1). For the actual transference of $\mathbf{x}_n = (\mathbf{x}_{n,1}, \dots, \mathbf{x}_{n,d})^* \in \mathbb{R}^d$, we define $X_{\boldsymbol{\eta}}: \mathbb{R}^d \rightarrow \mathbb{B}_d^N$ with $\boldsymbol{\eta} = (\boldsymbol{\eta}_1, \dots, \boldsymbol{\eta}_d)^* \in \mathbb{C}_d$ via

$$X_{\boldsymbol{\eta}}(\mathbf{x}_n) := (\chi_{\boldsymbol{\eta}_i}(\mathbf{x}_{n,i}))_{i=1}^d \quad \text{with} \quad \chi_{\boldsymbol{\eta}_i}(\mathbf{x}_{n,i}) := \begin{cases} 1 & \text{if } \mathbf{x}_{n,i} > \boldsymbol{\eta}_i, \\ -1 & \text{if } \mathbf{x}_{n,i} \leq \boldsymbol{\eta}_i. \end{cases}$$

Moreover, we introduce $X_{\boldsymbol{\eta}}(\mathbf{x}) := (X_{\boldsymbol{\eta}}(\mathbf{x}_n))_{n \in V}$ to transfer the entire signal. For the characteristic X , we obtain the following generalized version of [5, Lem. 3.1], which relates to the so-called coarea formula [15, 16].

Lemma 1. *For $\mathbf{x}_n, \mathbf{x}_m \in \mathbb{C}_d$, it holds*

$$\|\mathbf{x}_n - \mathbf{x}_m\|_1 = \frac{1}{2^d} \int_{\mathbb{C}_d} \|X_{\boldsymbol{\eta}}(\mathbf{x}_n) - X_{\boldsymbol{\eta}}(\mathbf{x}_m)\|_1 d\boldsymbol{\eta}.$$

Proof. For simplicity, we only consider the case $\mathbf{x}_{m,i} < \mathbf{x}_{n,i}$ for all $i \in \{1, \dots, d\}$ and obtain by Fubini's theorem

$$\int_{\mathbb{C}_d} \|X_{\boldsymbol{\eta}}(\mathbf{x}_n) - X_{\boldsymbol{\eta}}(\mathbf{x}_m)\|_1 d\boldsymbol{\eta} = 2^{d-1} \sum_{i=1}^d \int_{\mathbf{x}_{m,i}}^{\mathbf{x}_{n,i}} |1 - (-1)| d\boldsymbol{\eta}_i = 2^d \sum_{i=1}^d |\mathbf{x}_{m,i} - \mathbf{x}_{n,i}| = 2^d \|\mathbf{x}_n - \mathbf{x}_m\|_1.$$

The general case follows analogous. \square

Theorem 2. *Let $\mathbf{x}^* \in \mathbb{C}_d^N$ be a solution of (2). Then $X_{\boldsymbol{\eta}}(\mathbf{x}^*) \in \mathbb{B}_d^N$ is a solution of (1) for almost all $\boldsymbol{\eta} \in \mathbb{C}_d$.*

Proof. The proof follows ideas from [5, 11]. For any $\mathbf{x}_n \in \mathbb{C}_d^N$ and $\mathbf{y}_n \in \mathbb{R}^d$, we have the integral representation:

$$\begin{aligned} \frac{1}{2^d} \int_{\mathbb{C}_d^N} \langle X_{\boldsymbol{\eta}}(\mathbf{x}_n), \mathbf{y}_n \rangle d\boldsymbol{\eta} &= \frac{1}{2} \sum_{i=1}^d \int_{-1}^1 X_{\boldsymbol{\eta}_i}(\mathbf{x}_{n,i}) \mathbf{y}_{n,i} d\boldsymbol{\eta}_i = \frac{1}{2} \sum_{i=1}^d \left[\int_{-1}^{\mathbf{x}_{n,i}} \mathbf{y}_{n,i} d\boldsymbol{\eta}_i - \int_{\mathbf{x}_{n,i}}^1 \mathbf{y}_{n,i} d\boldsymbol{\eta}_i \right] \\ &= \frac{1}{2} \sum_{i=1}^d [\mathbf{x}_{n,i} - (-1) - (1 - \mathbf{x}_{n,i})] \mathbf{y}_{n,i} = \langle \mathbf{x}_n, \mathbf{y}_n \rangle. \end{aligned}$$

Together with Lem. 1, this yields

$$\begin{aligned}\mathcal{K}(\mathbf{x}^*) &= -\sum_{n \in V} \langle \mathbf{x}_n^*, \mathbf{y}_n \rangle + \lambda \sum_{(n,m) \in E} \|\mathbf{x}_n^* - \mathbf{x}_m^*\|_1 \\ &= \frac{1}{2^d} \int_{\mathbb{C}_d} \left[-\sum_{n \in V} \langle X_{\boldsymbol{\eta}}(\mathbf{x}_n^*), \mathbf{y}_n \rangle + \lambda \sum_{(n,m) \in E} \|X_{\boldsymbol{\eta}}(\mathbf{x}_n^*) - X_{\boldsymbol{\eta}}(\mathbf{x}_m^*)\|_1 \right] d\boldsymbol{\eta} = \frac{1}{2^d} \int_{\mathbb{C}_d} \mathcal{K}(X_{\boldsymbol{\eta}}(\mathbf{x}^*)) d\boldsymbol{\eta}.\end{aligned}$$

Since $\mathcal{K}(\mathbf{x}^{**}) \geq \mathcal{K}(\mathbf{x}^*)$ for any solution $\mathbf{x}^{**} \in \mathbb{B}_d^N$ of (1), $X_{\boldsymbol{\eta}}(\mathbf{x}^*)$ minimizes (1) for almost all $\boldsymbol{\eta} \in \mathbb{C}_d$ as well. \square

Solving the Convexified TV Model The convex problem (2) may be solved employing standard methods from convex analysis. Similarly to [5, § 3], we rely on the so-called Alternating Direction Method of Multipliers (ADMM) [4]. For this, we consider the splitting $\mathcal{K}(\mathbf{x}) + \iota_{\mathbb{C}_d}(\mathbf{u})$ with $\mathbf{x} - \mathbf{u} = 0$. Here, $\iota_{\mathbb{C}_d} \equiv 0$ on \mathbb{C}_d and $\iota_{\mathbb{C}_d} \equiv +\infty$ elsewhere. The proximal mapping of a general functional $\mathcal{F}: \mathbb{R}^{d \times N} \rightarrow \mathbb{R}$ and the projection onto a closed set $A \subset \mathbb{R}^{d \times N}$ are defined as

$$\text{prox}_{\mathcal{F}, \gamma}(\mathbf{z}) := \arg \min_{\mathbf{x} \in \mathbb{R}^{d \times N}} \left\{ \mathcal{F}(\mathbf{x}) + \frac{1}{2\gamma} \sum_{n \in V} \|\mathbf{x}_n - \mathbf{z}_n\|^2 \right\} \quad \text{and} \quad \text{proj}_A(\mathbf{z}) := \arg \min_{\mathbf{x} \in A} \sum_{n \in V} \|\mathbf{x}_n - \mathbf{z}_n\|^2.$$

Exploiting the computation rule for the proximal mapping, we obtain Algorithm 3.

Algorithm 3. ADMM to solve (2). Choose $\mathbf{x}^{(0)} = \mathbf{u}^{(0)} = \mathbf{z}^{(0)} = \mathbf{0} \in \mathbb{R}^N$, step size $\rho > 0$, and regularization parameter $\lambda > 0$

For $i \in \mathbb{N}$ **do:**

$$\begin{aligned}\mathbf{x}^{(i+1)} &= \text{prox}_{\mathcal{K}, \frac{1}{\rho}}(\mathbf{u}^{(i)} - \mathbf{z}^{(i)}) = \text{prox}_{\text{TV}, \frac{\lambda}{\rho}}(\mathbf{u}^{(i)} - \mathbf{z}^{(i)} + \frac{1}{\rho} \mathbf{y}) \\ \mathbf{u}^{(i+1)} &= \text{prox}_{\mathbb{C}_d^N, \frac{1}{\rho}}(\mathbf{x}_n^{(i+1)} + \mathbf{z}_n^{(i)}) = \text{proj}_{\mathbb{C}_d^N}(\mathbf{x}_n^{(i+1)} + \mathbf{z}_n^{(i)}) \\ \mathbf{z}^{(i+1)} &= \mathbf{z}^{(i)} + \mathbf{x}^{(i+1)} - \mathbf{u}^{(i+1)}\end{aligned}$$

Remark 4. The numerical projection to \mathbb{C}_d^N is unproblematic. Since we rely on an anisotropic TV regularization, the TV proximal mapping can be efficiently computed by applying the fast TV program [12] coordinatewise. The convergence of Algorithm 3 is guaranteed by [4, Cor. 28.3].

3 Denoising Stiefel-Valued Data

The (real) Stiefel-manifold $\mathbb{V}_d(k)$ is the union of all k -tuples of orthonormal vectors in \mathbb{R}^d with respect to the Euclidean inner product. In other words, $\mathbb{V}_d(k)$ consists of all orthonormal bases of all k -dimensional subspaces, where the order of a basis matter. Henceforth, we parametrize the Stiefel manifold as

$$\mathbb{V}_d(k) := \{\mathbf{X} \in \mathbb{R}^{d \times k} : \mathbf{X}^* \mathbf{X} = \mathbf{I}_k\},$$

where \mathbf{I}_k denotes the identity in $\mathbb{R}^{k \times k}$, and where the columns correspond to the basis vectors. We equip $\mathbb{R}^{d \times k}$ with the Euclidean geometry, i.e., with $\|\mathbf{X}\|_{\text{F}} := \sum_{j=1}^k \|\mathbf{x}_j\|^2$ and $\langle \mathbf{X}, \mathbf{Y} \rangle_{\text{F}} := \sum_{j=1}^k \langle \mathbf{x}_j, \mathbf{y}_j \rangle$ where $\mathbf{X} = [\mathbf{x}_1 | \dots | \mathbf{x}_k], \mathbf{Y} = [\mathbf{y}_1 | \dots | \mathbf{y}_k] \in \mathbb{R}^{d \times k}$. Moreover, we employ the 1-1-norm $\|\mathbf{X}\|_{1,1} := \sum_{j=1}^k \|\mathbf{x}_j\|_1$, the spectral norm $\|\mathbf{X}\|_2$, and the rank $\text{rk}(\mathbf{X})$. In order to denoise Stiefel-valued data, we use similar techniques as introduced in [5, 7]. More precisely, we propose a TV model for cartoon-like signals and a Tikhonov model for smooth signals. For the special case $\mathbb{V}_d(1) \simeq \mathbb{S}_{d-1}$, the proposed denoisers coincide with those in [5, 7].

3.1 TV Denoiser for Stiefel-Valued Data

To restore piecewise constant Stiefel-valued data $\mathbf{X} := (\mathbf{X}_n)_{n \in V} \in (\mathbb{V}_d(k))^N$ from noisy measurements $\mathbf{Y} := (\mathbf{Y}_n)_{n \in V} \in (\mathbb{R}^{d \times k})^N$, we consider the non-convex TV model:

$$\arg \min_{\mathbf{X} \in \mathbb{V}_d^N(k)} \frac{1}{2} \sum_{n \in V} \|\mathbf{X}_n - \mathbf{Y}_n\|_{\text{F}}^2 + \lambda \text{TV}(\mathbf{X}), \quad \text{where} \quad \text{TV}(\mathbf{X}) := \sum_{(n,m) \in E} \|\mathbf{X}_n - \mathbf{X}_m\|_{1,1}, \quad (3)$$

which relies on an anisotropic TV regularization on the ambient space $\mathbb{R}^{d \times k}$. In analogy to § 2, using $\frac{1}{2} \|\mathbf{X}_n - \mathbf{Y}_n\|_{\text{F}}^2 = -\langle \mathbf{X}_n, \mathbf{Y}_n \rangle_{\text{F}} + \text{constant}$, the objective may be replaced by

$$\mathcal{K}(\mathbf{X}) := - \sum_{n \in V} \langle \mathbf{X}_n, \mathbf{Y}_n \rangle_{\text{F}} + \lambda \text{TV}(\mathbf{X}).$$

For convexifying (3), we encode the non-convex domain by a series of positive semi-definite, fixed-rank matrices, where the rank constraint is relaxed afterwards. This procedure is inspired by similar considerations for hyperbolic-valued data [6].

Lemma 5. *Let $n \in V$ and $\mathbf{X}_n \in \mathbb{R}^{d \times k}$. Then $\mathbf{X}_n \in \mathbb{V}_d(k)$ if and only if $\mathbf{V}_n := \begin{bmatrix} \mathbf{I}_d & \mathbf{X}_n \\ \mathbf{X}_n^* & \mathbf{I}_k \end{bmatrix} \succeq \mathbf{0}$ and $\text{rk}(\mathbf{V}_n) = d$.*

Proof. If $\text{rk}(\mathbf{V}_n) = d$, then the last k rows of \mathbf{V}_n can be written as linear combinations of the independent first d rows. Based on this observation, we obtain the (positive semi-definite) low-rank representation

$$\mathbf{V}_n = \begin{bmatrix} \mathbf{I}_d \\ \mathbf{X}_n^* \end{bmatrix} \begin{bmatrix} \mathbf{I}_d & \mathbf{X}_n \end{bmatrix} = \begin{bmatrix} \mathbf{I}_d & \mathbf{X}_n \\ \mathbf{X}_n^* & \mathbf{X}_n^* \mathbf{X}_n \end{bmatrix} \quad \text{such that} \quad \mathbf{X}_n^* \mathbf{X}_n = \mathbf{I}_k \quad \text{and} \quad \mathbf{X}_n \in \mathbb{V}_d(k).$$

The other way round, if $\mathbf{X}_n \in \mathbb{V}_d(k)$, this representation implies $\text{rk}(\mathbf{V}_n) = d$ and $\mathbf{V} \succeq \mathbf{0}$. \square

Lemma 6. $\mathbf{V}_n \succeq \mathbf{0}$ if and only if $\|\mathbf{X}_n\|_2 \leq 1$.

Proof. Applying Schur's theorem [18, p. 495] to \mathbf{V}_n with respect to the upper left identity \mathbf{I}_d yields

$$\mathbf{V}_n \succeq \mathbf{0} \iff \mathbf{V}_n / \mathbf{I}_d = \mathbf{I}_k - \mathbf{X}_n^* \mathbf{X}_n \succeq \mathbf{0} \iff \mathbf{X}_n^* \mathbf{X}_n \preceq \mathbf{I}_k \iff \|\mathbf{X}_n\|_2 \leq 1. \quad \square$$

The non-convex TV model (3) may now be convexified by encoding the domain in $(\mathbf{V}_n)_{n \in V}$ via Lemma 5, relaxing the constraints on \mathbf{V}_n by neglecting the rank, and applying Lemma 6. This procedure yields the **convexified TV model**:

$$\arg \min_{\mathbf{X} \in (\mathbb{R}^{d \times k})^N} \mathcal{K}(\mathbf{X}) \quad \text{s.t.} \quad \|\mathbf{X}_n\|_2 \leq 1 \quad \forall n \in V. \quad (4)$$

Solving the Convexified TV-Model Basically, the convex minimization problem (4) can again be solved using ADMM [4], cf. § 2. More precisely, relying on the splitting $\mathcal{K}(\mathbf{X}) + \iota_{\mathbb{S}_{d,k}^N}(\mathbf{U})$ with $\mathbf{X} - \mathbf{U} = \mathbf{0}$, where $\mathbb{S}_{d,k}$ denotes the unit ball in $\mathbb{R}^{d \times k}$ with respect to the spectral norm, we obtain Algorithm 7.

Algorithm 7. ADMM to solve (4). Choose $\mathbf{X}^{(0)} = \mathbf{U}^{(0)} = \mathbf{Z}^{(0)} = \mathbf{0} \in (\mathbb{R}^{d \times k})^N$, step size $\rho > 0$, and regularization parameter $\lambda > 0$

For $i \in \mathbb{N}$ do:

$$\begin{aligned} \mathbf{X}^{(i+1)} &= \text{prox}_{\mathcal{K}, \frac{1}{\rho}}(\mathbf{U}^{(i)} - \mathbf{Z}^{(i)}) = \text{prox}_{\text{TV}, \frac{\lambda}{\rho}}(\mathbf{U}^{(i)} - \mathbf{Z}^{(i)} + \frac{1}{\rho} \mathbf{Y}) \\ \mathbf{U}^{(i+1)} &= \text{prox}_{\iota_{\mathbb{S}_{d,k}^N}, \frac{1}{\rho}}(\mathbf{X}_n^{(i+1)} + \mathbf{Z}_n^{(i)}) = \text{proj}_{\mathbb{S}_{d,k}^N}(\mathbf{X}_n^{(i+1)} + \mathbf{Z}_n^{(i)}) \\ \mathbf{Z}^{(i+1)} &= \mathbf{Z}^{(i)} + \mathbf{X}^{(i+1)} - \mathbf{U}^{(i+1)} \end{aligned}$$

Remark 8. It is well known that the projection onto $\mathbb{S}_{d,k}$ can be computed using an eigenvalue decomposition and projecting the eigenvalues therein onto $[-1, 1]$, similar to [7, Thm. 13]. Similarly to § 2, the TV proximal mapping can be efficiently computed by applying the fast TV program [12] coordinatewise. The convergence of Algorithm 7 is again guaranteed by [4, Cor. 28.3].

3.2 Tikhonov Denoiser for Stiefel-Valued Data

To restore smooth Stiefel-valued data $\mathbf{X} := (\mathbf{X}_n)_{n \in V} \in \mathbb{V}_d^N(k)$ from noisy measurements $\mathbf{Y} := (\mathbf{Y}_n)_{n \in V} \in (\mathbb{R}^{d \times k})^N$, we instead consider the non-convex Tikhonov model:

$$\arg \min_{\mathbf{X} \in \mathbb{V}_d^N(k)} \frac{1}{2} \sum_{n \in V} \|\mathbf{X}_n - \mathbf{Y}_n\|_{\text{F}}^2 + \frac{\lambda}{2} \sum_{n \in V} \|\mathbf{X}_n - \mathbf{X}_m\|_{\text{F}}^2. \quad (5)$$

Exploiting that, for $\mathbf{X}_n, \mathbf{X}_m \in \mathbb{V}_d(k)$ and fixed $\mathbf{Y}_n \in \mathbb{R}^{d \times k}$, $\|\mathbf{X}_n - \mathbf{Y}_n\|_F = -\langle \mathbf{X}_n, \mathbf{Y}_n \rangle_F + \text{constant}$ and $\|\mathbf{X}_n - \mathbf{X}_m\|_F = -\langle \mathbf{X}_n, \mathbf{X}_m \rangle_F + \text{constant}$, and introducing the auxiliary variables $\mathbf{L}_{(n,m)} := \mathbf{X}_n^* \mathbf{X}_m$, we rewrite the objective of (5) using

$$\mathcal{L}(\mathbf{X}, \mathbf{L}) := -\sum_{n \in V} \langle \mathbf{X}_n, \mathbf{Y}_n \rangle_F - \sum_{(n,m) \in E} \langle \mathbf{L}_{(n,m)}, \mathbf{1}_k \rangle_F,$$

where $\mathbf{1}_k \in \mathbb{R}^{k \times k}$ denotes the all-one matrix. In analogy to [7] for sphere-valued data, we encode the non-convex domain $\mathbf{X}_n \in \mathbb{V}_d(k)$ and the non-convex side condition $\mathbf{L}_{(n,m)} := \mathbf{X}_n^* \mathbf{X}_m$ using positive semi-definite, fixed-rank matrices.

Lemma 9. *Let $\mathbf{X}_n, \mathbf{X}_m \in \mathbb{R}^{d \times k}$ and $\mathbf{L}_{(n,m)} \in \mathbb{R}^{k \times k}$. Then $\mathbf{X}_n, \mathbf{X}_m \in \mathbb{V}_d(k)$ and $\mathbf{L}_{(n,m)} := \mathbf{X}_n^* \mathbf{X}_m$ if and only if*

$$\mathbf{Q}_{(n,m)} := \begin{bmatrix} \mathbf{I}_d & \mathbf{X}_n & \mathbf{X}_m \\ \mathbf{X}_n^* & \mathbf{I}_k & \mathbf{L}_{(n,m)} \\ \mathbf{X}_m^* & \mathbf{L}_{(n,m)}^* & \mathbf{I}_k \end{bmatrix} \succeq \mathbf{0} \quad \text{and} \quad \text{rk}(\mathbf{Q}_{(n,m)}) = d.$$

The lemma can be proven like Lemma 5 by considering the decomposition

$$\mathbf{Q}_{(n,m)} = [\mathbf{I}_d, \mathbf{X}_n, \mathbf{X}_m]^* [\mathbf{I}_d, \mathbf{X}_n, \mathbf{X}_m].$$

Removing the rank constraint regarding $\mathbf{Q}_{(n,m)}$, we propose to solve the **convexified Tikhonov model**:

$$\arg \min_{\substack{\mathbf{X} \in (\mathbb{R}^{d \times k})^N \\ \mathbf{L} \in (\mathbb{R}^{k \times k})^M}} \mathcal{L}(\mathbf{X}, \mathbf{L}) \quad \text{s.t.} \quad \mathbf{Q}_{(n,m)} \succeq \mathbf{0} \quad \forall (n, m) \in E. \quad (6)$$

Solving the Convexified Tikhonov Model To handle the positive semi-definiteness constraints on $\mathbf{Q}_{(n,m)}$ jointly, we introduce the linear operator $\mathcal{Q} := (\mathcal{Q}_{(n,m)})_{(n,m) \in E}$ with

$$\mathcal{Q}_{(n,m)} : (\mathbb{R}^{d \times k})^N \times (\mathbb{R}^{k \times k})^M \rightarrow \mathbb{R}^{(d+2k) \times (d+2k)}, \quad (\mathbf{X}, \mathbf{L}) \mapsto \mathbf{Q}_{(n,m)} - \mathbf{I}_{d+2k}$$

and denote the restriction of its adjoint to the argument \mathbf{X} by $\mathcal{Q}_{\mathbf{X}}^*$ as well as to \mathbf{L} by $\mathcal{Q}_{\mathbf{L}}^*$. To solve (6), we apply the ADMM [4] to the splitting $\mathcal{L}(\mathbf{X}, \mathbf{L}) + \iota_{\mathbb{P}_{d+2k}^M}(\mathbf{U})$ with $\mathbf{U} = \mathcal{Q}(\mathbf{X}, \mathbf{L})$ and $\mathbb{P}_{d+2k} := \{\mathbf{A} \in \mathbb{R}^{(d+2k) \times (d+2k)} : \mathbf{A} \succeq -\mathbf{I}_{d+2k}\}$. Relying on similar arguments as in the proof of [7, Thm. 5.1], a brief direct calculation yields Algorithm 10, where the number of connected vertices is defined as $\nu_n := |\{m \in V : (n, m) \in E \vee (m, n) \in E\}|$.

Algorithm 10. ADMM to solve (6). Choose $\mathbf{X}^{(0)} = \mathbf{0} \in (\mathbb{R}^{d \times k})^N$ and $\mathbf{U}^{(0)} = \mathbf{Z}^{(0)} = \mathbf{0} \in (\mathbb{R}^{k \times k})^M$, step size $\rho > 0$ and regularization parameter $\lambda > 0$

For $i \in \mathbb{N}$ **do:**

$$\begin{aligned} \mathbf{X}_n^{(i+1)} &= \frac{1}{2\nu_n} [\mathcal{Q}_{\mathbf{X}}^*(\mathbf{U}^{(i)} - \mathbf{Z}^{(i)})_n + \frac{1}{\rho} \mathbf{Y}_n] \quad \forall n \in V \\ \mathbf{L}_{(n,m)}^{(i+1)} &= \frac{1}{2} [\mathcal{Q}_{\mathbf{L}}^*(\mathbf{U}^{(i)} - \mathbf{Z}^{(i)})_{(n,m)} + \frac{\lambda}{\rho} \mathbf{E}] \quad \forall (n, m) \in E \\ \mathbf{U}_{(n,m)}^{(i+1)} &= \text{proj}_{\mathbb{P}_{d+2k}}(\mathcal{Q}_{(n,m)}(\mathbf{X}^{(i+1)}, \mathbf{L}^{(i+1)}) + \mathbf{Z}_{(n,m)}^{(i)}) \quad \forall (n, m) \in E \\ \mathbf{Z}^{(i+1)} &= \mathbf{Z}^{(i)} + \mathcal{Q}(\mathbf{X}^{(i+1)}, \mathbf{L}^{(i+1)}) - \mathbf{U}^{(i+1)} \end{aligned}$$

Remark 11. The projection onto \mathbb{P}_{d+2k} can be computed using an eigenvalue decomposition and projecting the eigenvalues therein onto $[-1, \infty)$. The convergence of Algorithm 10 is again guaranteed by [4, Cor. 28.3].

4 Numerical Results

All algorithms are implemented¹ in Python 3.11.9 using Numpy 1.25.0 and Scipy 1.11.1. The following experiments are performed on an off-the-shelf MacBook Pro 2020 with Intel Core i5 Chip (4-Core CPU, 1.4 GHz) and 8 GB RAM. In every experiment, we use a range of regularization parameters and finally choose the parameter yielding the smallest mean squared error (MSE) in sense of the restoration.

¹The code is available at GitHub https://github.com/JJEWBresch/relaxed_tikhonov_regularization.

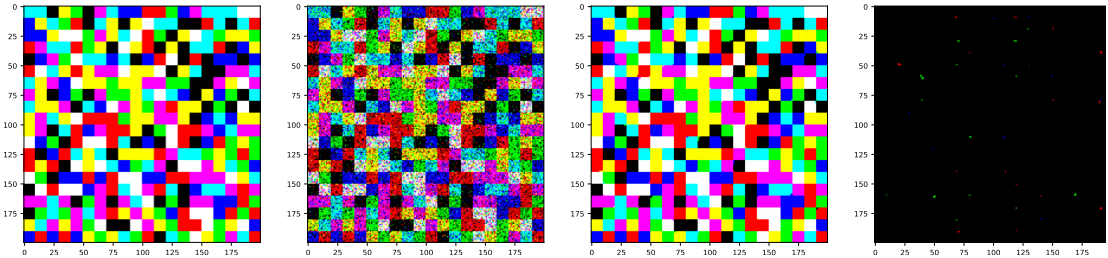


Figure 1: Multi-color QR code denoising (from left to right): ground truth (first), corrupted image by (3-dimensional) Gaussian noise with standard deviation $\sqrt{2} \cdot 0.5$ (second), restoration using Algorithm 3 with $\lambda = 1.2, \rho = 0.1$ (third), and the restoration error (forth). The mean absolute distance of the restored pixels to \mathbb{B}_3 is in order of 10^{-5} , i.e., here Algorithm 3 actually yields a solution of the non-convex TV model (1) without the projection procedure outlined in Theorem 2.

Multi-Binary-Valued Data A real-world application for multi-binary data denoising is the restoration of multi-color QR codes [28]. Figuratively, these QR codes are generated by combining three independent QR codes in the RGB (red-green-blue) color space. The modules of the resulting QR codes are then colored in black, red, green, blue, cyan, magenta, yellow, and white—corresponding to the vertices of the RGB color space. To fit our setting, we scale and shift the RGB color space such that the module colors can be interpreted as \mathbb{B}_3 data. For a proof-of-concept, we employ a 20×20 , multi-color QR code that is distorted by independent, 3-dimensional Gaussian noise on a 10-times finer grid, yielding an \mathbb{R}^3 -valued image. The ground truth and the noisy multi-color QR code are reported in Figure 1 (first, second). Applying Algorithm 3, we obtain the restored multi-color QR code in Figure 1 (third). Interestingly, Algorithm 3 already yields a \mathbb{B}_3 -valued restoration; therefore, the projection procedure outlined in Theorem 2 is here not required. Although we here have to deal with severe noise, the reconstruction is nearly perfect up to some single pixels.

Stiefel-Valued Data For a proof of concept, we study the TV model (4) and the Tikhonov model (6) for a synthetic $\mathbb{V}_3(2)$ -valued signal of length 200. Our ground truth is reported in Figure 2 (left). The vectors in the orthogonal bases are then distorted using the von Mises–Fischer distribution and are reorthonormalized employing the Gram–Schmidt process. The resulting $\mathbb{V}_3(2)$ -valued noisy signal is reported in Figure 2 (middle left). To remove the noise, we apply our proposed convexified TV model (Algorithm 7) and Tikhonov model (Algorithm 10). The restored $\mathbb{V}_3(2)$ -signals are reported in Fig. 2 (middle right, right). For both models, we observe convergence to the Stiefel manifold in the sense that the norm of basis vectors in $\mathbf{X}_n^{(i)}$ converges to one and that the inner product of the basis vectors converges to zero. Consequently, both algorithms here actually yield minimizers of the non-convex TV model (3) and Tikhonov model (5), respectively. Especially, the Tikhonov model nearly recovers the ground truth.

References

- [1] B. L. Adams, S. I. Wright, and K. Kunze. Orientation imaging: the emergence of a new microscopy. *Metall. Mater. Trans. A*, 24:819–831, 1993.
- [2] I. F. Anderson. Advanced QR Code Generator with RGB Color Method in Python to Expand Data Capacity. *J. Sen. Net. Data Comm.*, 4(2):1–20, 08 2024.
- [3] F. Bachmann, R. Hielscher, P. E. Jupp, W. Pantleon, H. Schaeben, and E. Wegert. Inferential statistics of electron backscatter diffraction data from within individual crystalline grains. *J. Appl. Crystallogr.*, 43:1338–1355, 2010.

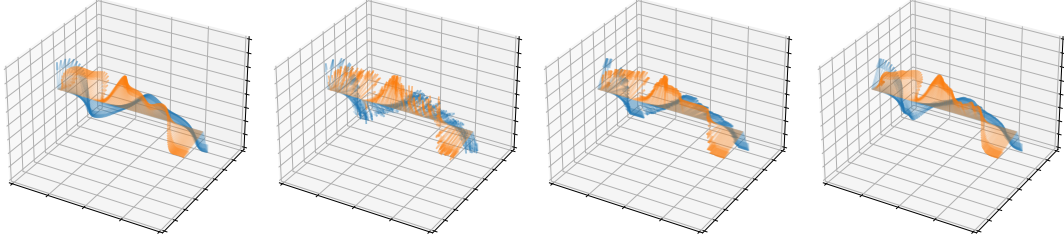


Figure 2: Restoration of a $\mathbb{V}_3(2)$ -valued signal (from left to right): ground truth (left), noisy measurement (middle left), restored signal using Algorithm 7 (convexified TV model) with $\lambda = 0.75, \rho = 0.5$ (middle right), and using Algorithm 10 (convexified Tikhonov model) with $\lambda = 10, \rho = 0.1$ (right). In both cases the mean absolute distance of the norm of the recovered basis vectors to one is of order 10^{-5} , the mean absolute distance of the inner product between the recovered basis vectors to zero is of order 10^{-4} .

- [4] H. H. Bauschke and P. L. Combettes. *Convex Analysis and Monotone Operator Theory in Hilbert Spaces*. Springer, Cham, 2017.
- [5] R. Beinert and J. Bresch. Denoising sphere-valued data by relaxed total variation regularization. *Proc. Appl. Math. Mech.*, 24(1):e202400016, 2024.
- [6] R. Beinert and J. Bresch. Denoising Hyperbolic-Valued Data by Relaxed Regularizations. In *Proceedings SSVM '25, Dartington, UK*, pages 16–29, Cham, 2025. Springer.
- [7] R. Beinert, J. Bresch, and G. Steidl. Denoising of sphere- and $\text{SO}(3)$ -valued data by relaxed Tikhonov regularization. *Inverse Probl. Imaging*, 19(1):87–108, 2025.
- [8] R. Bergmann, R. H. Chan, R. Hielscher, J. Persch, and G. Steidl. Restoration of manifold-valued images by half-quadratic minimization. *Inverse Probl. Imaging*, 10(2):281–304, 2016.
- [9] R. Bergmann, F. Laus, G. Steidl, and A. Weinmann. Second order differences of cyclic data and applications in variational denoising. *SIAM J. Imaging Sci.*, 7(4):2916–2953, 2014.
- [10] R. Bergmann, J. Persch, and G. Steidl. A parallel Douglas-Rachford algorithm for minimizing ROF-like functionals on images with values in symmetric Hadamard manifolds. *SIAM J. Imaging Sci.*, 9(3):901–937, 2016.
- [11] R. Choksi, Y. van Gennip, and A. Oberman. Anisotropic Total Variation Regularized L^1 -Approximation and Denoising/Deblurring of 2D Bar Codes. *Inverse Probl. Imaging*, 5(3):591–617, 2011.
- [12] L. Condat. A Direct Algorithm for 1D Total Variation Denoising. *IEEE Signal Process. Lett.*, 20(11):1054–1057, 2013.
- [13] D. Cremers and E. Strekalovskiy. Total cyclic variation and generalizations. *J. Math. Imaging Vis.*, 47(3):258–277, 2013.
- [14] A. Edelman, T. A. Arias, and S. T. Smith. The geometry of algorithms with orthogonality constraints. *SIAM J. Matrix Anal. Appl.*, 20(2):303–353, 1998.
- [15] H. Federer. Curvature measures. *Trans. Am. Math. Soc.*, 93(3):418–491, 1959.
- [16] W. H. Fleming and R. Rishel. An integral formula for total gradient variation. *Arch. Math.*, 11(1):218–222, 1960.
- [17] P. Grohs and M. Sprecher. Total variation regularization on Riemannian manifolds by iteratively reweighted minimization. *Inf. Inference*, 5(4):353–378, 2016.
- [18] R. A. Horn and C. R. Johnson. *Matrix Analysis*. Cambridge University Press, Cambridge, 2nd edition, 2012.

- [19] R. Kenis, E. Laude, and P. Patrinos. arXiv:2308.00079, 2023.
- [20] T. Lan, D. Erdogmus, S. J. Hayflick, and J. U. Szumowski. Phase unwrapping and background correction in MRI. In *Proceedings MLSP '08, Cancun, Mexico*, pages 239–243, New York, 2008. IEEE.
- [21] F. Laus, M. Nikolova, J. Persch, and G. Steidl. A nonlocal denoising algorithm for manifold-valued images using second order statistics. *SIAM J. Imaging Sci.*, 10(1):416–448, 2017.
- [22] J. Lee. *Riemannian Manifolds: An Introduction to Curvature*. Springer, New York, 1997.
- [23] J. Lellmann, E. Strekalovskiy, S. Koetter, and D. Cremers. Total variation regularization for functions with values in a manifold. In *Proceedings ICCV '13, Sydney, Australia*, pages 2944–2951, New York, 2013. IEEE.
- [24] P. Mishra. *Region Identification and Decoding Of Security Markers Using Image Processing Tools*. PhD thesis, 2016.
- [25] M. Nikolova and G. Steidl. Fast hue and range preserving histogram specification: theory and new algorithms for color image enhancement. *IEEE Trans. Image Process.*, 23(9):4087–4100, 2014.
- [26] J. Persch, F. Pierre, and G. Steidl. Exemplar-based face colorization using image morphing. *J. Imaging*, 3(4):48, 2017.
- [27] M. H. Quang, S. H. Kang, and T. M. Le. Image and video colorization using vector-valued reproducing kernel Hilbert spaces. *J. Math. Imaging Vis.*, 37:49–65, 2010.
- [28] L. Tan, K. Liu, X. Yan, S. Wan, J. Chen, and C. Chang. Visual secret sharing scheme for color qr code. In *Proceedings ICIVC '18, Chongqing, China*, pages 961–965, New York, 2018. IEEE.
- [29] P. Turaga, A. Veeraraghavan, A. Srivastava, and R. Chellappa. Statistical computations on grassmann and stiefel manifolds for image and video-based recognition. *IEEE Trans. Pattern Anal. Mach. Intell.*, 33(11):2273–2286, 2011.
- [30] Z. Wen and W. Yin. A feasible method for optimization with orthogonality constraints. *Math. Program.*, 142:397–434, 2013.